Nanoscale Advances

ROYAL SOCIETY OF CHEMISTRY

PAPER

View Article Online
View Journal | View Issue

Cite this: *Nanoscale Adv.*, 2021, **3**, 4271

Photoluminescence investigations of sulfur quantum dots synthesized by a bubbling-assisted strategy†

Shuo Liu,‡[a] Henggang Wang,‡[a] Anrui Feng,[a] Jianyu Chang,[a] Chuanchuan Zhang,[a] Yu-e Shi,*[a] Yongqing Zhai,[a] Vasudevanpillai Biju *[b] and Zhenguang Wang *[a]

Received 17th April 2021
Accepted 19th June 2021

DOI: 10.1039/d1na00282a

rsc.li/nanoscale-advances

Sulfur quantum dots (S-dots) emerge as promising luminescent materials owing to their remarkable optical properties. However, the mechanisms of their formation and photoluminescence remain concealed. We reveal these mechanisms by the bubbling-assisted synthesis and spectroscopic study of S-dots formed from sulfur ions produced by the alkaline oxidation of bulk sulfur under the passivation of PEG. The emission colour of the S-dots depends on the size, explained by the quantum confinement effect. The dots' luminescent quantum efficiency is strongly affected by the surface sulfur species, which is optimized by the proper surface oxidation. The simple synthesis, excellent luminescence properties, and metal-free nature attract S-dots to optoelectronic and electroluminescence applications.

Introduction

Sulfur quantum dots (S-dots) are an emerging class of zero-dimensional luminescent material free from metal ions. These dots show bright photoluminescence (PL), tunable emission color, and strong absorption in the UV-vis region.[1–3] Furthermore, their facile synthesis, low toxicity, favourable biocompatibility, and unique optical properties attract widespread attention in chemistry, materials science, and physics. Moreover, by revealing the structure–property relations, S-dots can be extended to areas such as chemical sensing, nanomedicine, and photocatalysis. To-date the properties of S-dots are explained in the framework of the quantum confinement in semiconductor nanocrystals.[4–6] For example, based on the size-dependent PL properties, blue and green emissions are reported for S-dots passivated with polyethylene glycol (PEG). Like semiconductor quantum dots (QDs), the emission color of S-dots blueshifts with decreasing particle size.[7,8] However, distinct differences from traditional chalcogenide QDs are relatively broad emission bands, excitation energy-dependent emission maximum, and short PL lifetimes.[9–11] These phenomena suggest that the quantum confinement theory is not fully applicable to explain their PL behaviours. Furthermore, the size and surface groups pose significant challenges to regulating the synthesis, surface structure, and size of S-dots and unveiling their emission mechanism.[12–14]

A top-down strategy through etching bulk elemental sulfur into quantum dots under the passivation of ligands is the most widely employed synthesis method, where assembling and fission of S-dots are involved and contest each other.[7,11,14] However, limited by the relatively long reaction time for reaching a dynamic equilibrium and the ultra-small energy barrier between the assembling and fission effect, the reaction mechanisms are complicated to characterize, let alone to study their fundamental emission mechanisms. Much effort was made to modulate the "assemble-fission" process.[1,13] Our group introduced ultrasonication treatment to prevent the assembling process, and luminescent S-dots was obtained within 10 h.[15] Zhou's group reported that providing the synthesis system with a pure oxygen atmosphere can change the reaction route by oxidizing polysulfide species into elemental sulfur.[16] Although these approaches accelerated the synthesis of monodispersed S-dots with excellent luminescence properties, the severe oxidation–reduction conditions prevented the characterization of reaction intermediates and concealed the relationships between the interfacial/surface structure and S-dots' PL properties.[16,17]

In this work, well-dispersed luminescent S-dots are synthesized by a mild bubbling-assisted strategy, which offers an alternative to tune the S-dot surface properties. The bulk sulfur was etched into S^{2-} and polysulfide by NaOH. S-dots were formed after oxidation of S^{2-} and polysulfide into elemental sulfur, under the passivation of PEG. S-dots' emission is proved to be the synergistic contribution of the size, surface species, and organic emitters. The emission colour depends on the size,

[a]*Key Laboratory of Chemical Biology of Hebei Province, Key Laboratory of Medicinal Chemistry and Molecular Diagnosis, Ministry of Education, College of Chemistry & Environmental Science, Hebei University, Baoding 071002, China. E-mail: zwang65-c@my.cityu.edu.hk*

[b]*Graduate School of Environmental Science, Hokkaido University, N10 W5, Sapporo, Hokkaido 060-0810, Japan*

† Electronic supplementary information (ESI) available. See DOI: 10.1039/d1na00282a

‡ Those authors contribute equally.

well explained by the classical theory of quantum confinement. The luminescence intensity is strongly affected by the surface sulfur species (S^{2-} and S_x^{2-}), and proper oxidation of those species improves the PL quantum efficiency. The bubbled oxygen was critical for forming luminescent S-dots by transferring divalent sulfur ions into the elemental sulfur core and etching the particle surface to inhibit nonradiative relaxations.

Results and discussion

Sublimed sulfur powder (1.4 g), PEG (3.0 mL), and sodium hydroxide (4.0 g) were dissolved in 50 mL water in a flask, which was equipped with an air pump to keep the ventilation of the reaction system. The mixture was heated at 70 °C under continuous stirring. The yellow sulfur powder gradually dissolved into an aqueous solution with orange-red color, and the extension of heating and bubbling time decreased the solution colour. A weak green emission appeared after 5 h, indicating the formation of S-dots. The as-obtained S-dots were well-dispersed in an aqueous solution. As indicated by the TEM images (Fig. 1a), the S-dots were quasi-spherical in shape, with an average diameter of 5 nm. XPS measurements (Fig. 1b) were conducted to clarify the chemical composition of S-dots. XPS survey spectrum suggests that S-dots are composed of C, O and S (Fig. S1†). The doublet peaks located at 160.1 and 161.3 eV suggest the presence of divalent sulfur ions, attributed to S^{2-} and polysulfide (S_x^{2-}).[18,19] The intensive peak at 164.2 eV confirms elemental sulfur.[7] The binding energies at 166.3, 167.3 and 170.3 eV are assigned to oxidized sulfur composition of SO_3^{2-} ($2p_{3/2}$), SO_3^{2-} ($2p_{1/2}$), and SO_4^{2-} ($2p_{1/2}$), respectively.[12,20] The divalent sulfur ions and SO_3^{2-} should be produced by the reaction between NaOH and bulk sulfur, following reaction (1) and reaction (2).[21] The content of SO_4^{2-}, SO_3^{2-}, atomic sulfur, and divalent sulfur ions were 4.6%, 56.8%, 4.3%, and 34.3%, calculated from the fitted XPS spectra. The existence of SO_4^{2-}, nearly equal content with that of atomic sulfur, is produced through the oxidation of divalent sulfur ions by O_2 during the bubbling-assisted synthesis process, following reaction (3).[16] The S-dot composition was also studied by collecting the *in situ* Raman spectra collected at different reaction times (Fig. 1c). An intensive peak located at 450 cm^{-1} in all the S-dots samples come from elemental sulfur.[22,23] Two relatively weak bands at 981 and 999 cm^{-1}, originating from the ν_1 modes of the sulphate groups, become strong with increasing reaction time, suggesting the formation of SO_4^{2-} during the reaction, which is consistent with the XPS results.[24,25]

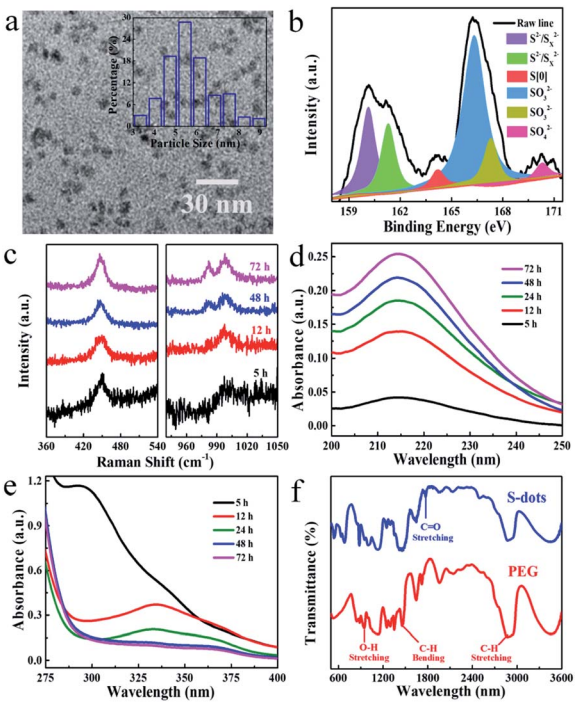

Fig. 1 (a) TEM image, with size distribution showing as insert, and (b) the high-resolution XPS spectra for S2p of S-dots. (c) Raman and (d and e) UV-visible absorption spectra of S-dots, obtained by different reaction times. (f) FTIR spectra of S-dots (blue line) and pure PEG (red line).

$$3S + 6NaOH = 2Na_2S + Na_2SO_3 + 3H_2O \quad (1)$$

$$(x-1)S + S^{2-} \rightarrow S_x^{2-} \quad (2)$$

$$S_x^{2-} + O_2 \rightarrow S + SO_3^{2-} + SO_4^{2-} \quad (3)$$

Also, the reactions mentioned above are confirmed by the time-dependent UV-visible absorption spectra of S-dots. To better resolving those spectral features, the UV-visible absorption spectra were recorded separately in the regions of 200–250 nm and 280–400 nm (Fig. 1d and e). After 5 h reaction, a prominent peak assigned to the n → σ* transition of nonbonding electrons on elemental sulfur was observed at 215 nm.[20,26] This peak became intense with time under the reaction. A strong peak at 298 nm, attributed to S_x^{2-}, was present during the 5 h reaction, the intensity of which decreased with time and disappeared after 12 h reaction.[19] While the peaks around 335 and 370 nm, attributed to the bandgap transitions of elemental sulfur and S_x^{2-}, appeared and became intense with the extension of reaction time.[24,27] These results suggest the formation of S_x^{2-} through reaction (1) and reaction (2), which is further oxidized into higher valance states by O_2, consistent with XPS results. *In situ* FTIR spectra of pure PEG and S-dots were collected to study the reaction process (Fig. 1f). Characteristic PEG peaks located at 2870, 945, and 1450 cm^{-1} are observed in those spectra, attributed to the stretching vibrations of C–H, and O–H, the bending vibration of C–H, respectively.[28,29] Also, an apparent peak in the range from 1730 to 1800 cm^{-1} was observed compared with pure PEG, attributed to ester absorption, formed through the oxidization of PEG by O_2. Several peaks in the short wavelength range (500 to 800 cm^{-1}) were recognized on the FTIR spectra of S-dots, characteristics of PEG fragments.[28] These results suggest that a portion of PEG is fragmented through oxidization by O_2.

Green fluorescence can be observed after reaction for 5 h, which is much shorter than previous work (30 h). This is caused by the high oxidation speed of S^{2-} and polysulfide into

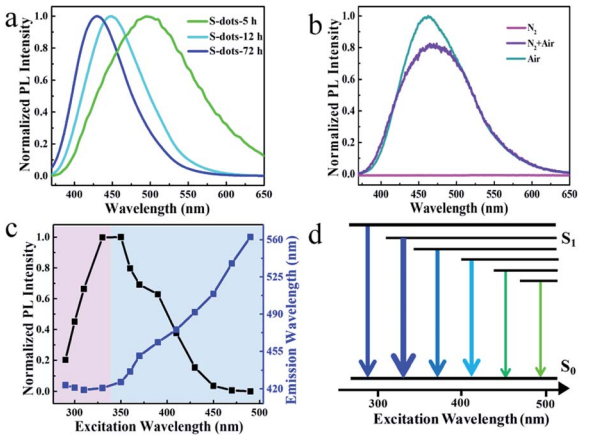

Fig. 2 (a) Normalized PL spectra of S-dots obtained by different reaction times, excited at 365 nm. (b) Normalized PL spectra of S-dots synthesized under the bubbling of different gas, excited 365 nm. (c) PL peak position (blue line) and normalized peak intensity (black line) as a function of the excitation wavelength of S-dots. (d) The simplified Jablonski diagrams of emission pathways.

elemental sulfur by the pumped air, compared with the low concentration of dissolved oxygen in water. The emission color can be tuned in the wavelength range from 425 to 500 nm by controlling the reaction time (Fig. 2a and S2†). The emission spectra are relatively broad compared with traditional QDs, and extension of reaction time results in the narrowing of the spectral width, from 144 nm to 80 nm.[6,30] Bubbling the reaction system with fresh air plays an essential role in the luminescent properties. Conversely, by bubbling the system with N_2, we failed to observe any luminescence even after 100 h reaction. In contrast, an intensive blue-green emission appeared after bubbling the non-emissive products with fresh air for several hours (Fig. 2b). These results confirm that O_2 is essential for the formation of luminescent S-dots. The TEM images and PL spectra of S-dots synthesized by different reaction time (5, 12, and 72 h) were recorded (Fig. S3†). The S-dots synthesized after reaction for 5 h are likely to aggregate and form large assembling particles, which is difficult to count the size of induvial S-dots. A rather weak green emission can be recorded. After extending the reaction time to 12 h, a clear boundary can be observed between S-dots, and an average size of 8.5 nm is calculated by counting the size of more than 200 dots. Compared with S-dots synthesized under 5 h, a blue shift of the peak and an obvious increase on the PL intensity are observed, with a PL maximum located at 450 nm. The S-dots obtained by reaction for 72 h are well dispersed, and an average diameter of 5 nm is recorded on the TEM image. Extension the reaction time to 72 h results in the narrowing of the spectral width (from 144 nm to 80 nm), and further increasing of PL intensity (Fig. S3†). A PL maximum located at 423 nm can be recorded. Thus, we conclude that extension of reaction time results in the decreasing of particles size of S-dots, which also leads to a blue shift of the peak and an obvious increase on the PL intensity.

The S-dots show excitation energy-dependent emission colour (Fig. S4†), which is further evaluated by comparing the PL peaks of S-dots at different excitation wavelengths (Fig. 2c). The trends are also illustrated by a simplified Jablonski diagram (Fig. 2d), which shows the changes of emission colour and intensities in correlation to the excitation wavelength. The arrow's thickness stands for the emission intensity, and its colour illustrates the emission wavelength. The excitation wavelength can be clearly divided into two separate regions. Under excitation in the wavelength range of 280 to 330 nm, the emission peak position is excitation energy-independent, with an identical peak located at 420 nm. The emission intensity increases sharply with increases in the excitation wavelength, and the highest intensity is achieved at the excitation wavelength of 330 nm. Shifting the excitation wavelength to a longer range leads to the PL peak redshift from 450 to 560 nm, quickly dropping the PL intensity to zero at the excitation wavelength beyond 450 nm (Fig. 2c). The PL QY is also excitation wavelength dependent. PL QY *ca.* 8% was measured in the 390–430 nm excitation range, which was decreased to 4% when excited below 370 nm (Fig. S5†). This change in PL QY suggests multiple emission species in the S-dot sample, showing different emission colours and QYs.

To further reveal the emission species, the PL excitation (PLE) spectra of S-dots were recorded and analyzed. The PLE spectra vary with the emission wavelengths in the range from 270 to 500 nm, and three excitation bands at 300, 350, and 390 nm were verified (Fig. 3a). Interestingly, the excitation

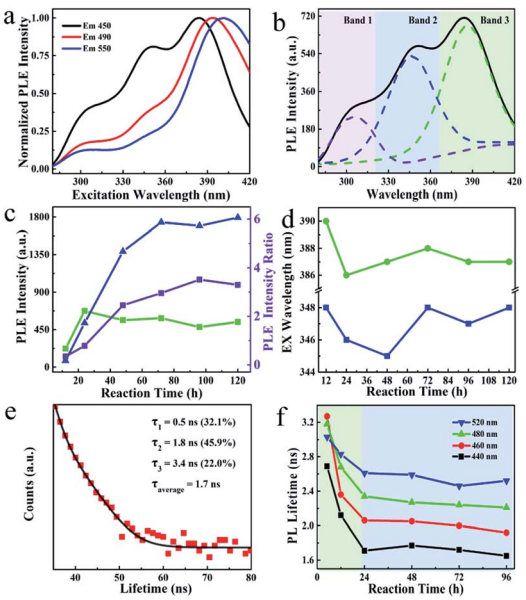

Fig. 3 (a) Normalized PLE spectra of S-dots recorded at different detection wavelengths, as indicated on the frame. (b) Deconvoluted PLE spectra of S-dots, detected at 450 nm. (c) PLE intensity of deconvoluted band 1 (blue line), band 2 (green line), and the ratio of the intensity (purple line). (d) PLE peak position of S-dots as the function of reaction time, recorded at 450 nm, as the function of reaction time. (e) Time-resolved PL decay curve of S-dots, with the fitting results showing as insert, excited at 410 nm, detected at 500 nm. (f) The PL lifetime is a function of the S-dots' excitation wavelength, recorded at different emission wavelengths, as indicated on the frames, excited at 410 nm.

transition is fixed at 300 nm for the PLE spectra detected at 450, 490, and 550 nm. The band located at 350 nm became relatively weak. In contrast, a noticeable enhancement in the intensity and a redshift (386 to 396 nm) of the peak position was observed for the band at 390 nm, after shifting the detection wavelength from 450 to 550 nm (Fig. 3a).

To verify the PLE bands, control experiments were conducted by heating a solution of PEG or PEG/NaOH. The PL and PLE spectra (Fig. S6†) of these samples suggest that the excitation transition at 300 nm can be attributed to the reaction product of PEG under alkaline conditions, recalling the partial oxidation of PEG revealed by the FTIR results. Thus, PEG is oxidized by O_2 under alkaline conditions, providing intense blue-emissive species, with PLE bands at 300 nm. Furthermore, we deconvoluted the PLE spectra into three peaks (Fig. 3b). The PLE bands are dominant by the peaks at 390 nm on the spectra of S-dots produced under a relatively low temperature (<60 °C), a short reaction time (<48 h), and a low dosage of NaOH (Fig. S7, S8, and S9†). Also, elevated reaction temperatures and prolonged reaction times increase the intensity of the broad PLE bands at 350 nm, with two shoulder peaks at 300 and 390 nm (Fig. 3c and d). These changes to the PLE bands are attributed to the size change of S-dots. Relatively large particles tend to form under low temperatures and a shortage of etching reagents, resulting in long-wavelength PL and PLE bands.[30] Conversely, small particles are thermodynamically favoured, and the excitation bands at shorter wavelengths become dominant. From the emission spectral blueshift with the extension of reaction time (Fig. 2a), we conclude that the excitation bands in the range 330–420 nm originate from the S-dots core, which show size-dependent properties. This behaviour is correlated with the excitation energy-dependent emission spectra, presented in Fig. S4,† which are attributed to the S-dot's size heterogeneity.

To further confirm the above mechanisms, time-resolved PL decays of S-dots synthesized during different reaction times showing different emission wavelengths were recoded (Fig. 3e and S10†). According to the classical theory of semiconductor QDs, the emission from surface states draws a long component in the PL decay profile. Conversely, small QDs always show a relatively short PL lifetime.[31–33] To verify such a size–lifetime relationship in the current work, we fitted the decay curves with the third-exponential functions. Interestingly, the average PL lifetime is increased with an increase in the detection wavelength (Fig. 3f, and Table S1†). This increase is related to the heterogeneity of the S-dots size, like conventional QDs. Although the PL lifetime was monotonously decreased during the 24 h reaction, it remained constant from 24 to 96 h (Fig. 3f). The initial decrease is attributed to the etching of surface states through oxidization of divalent sulfur ions by O_2, reducing the proportion of emission from surface states with a long lifetime. Besides, the etching of surface chemical groups increased the PL intensity by suppressing the nonradiative paths. This increase in intensity well-explains the phenomenon that S-dots synthesized under an N_2 atmosphere fails to emit any light (Fig. 2b). Here, most of the excitons are quenching by the chemical groups (divalent sulfur ions) around the S-dots.

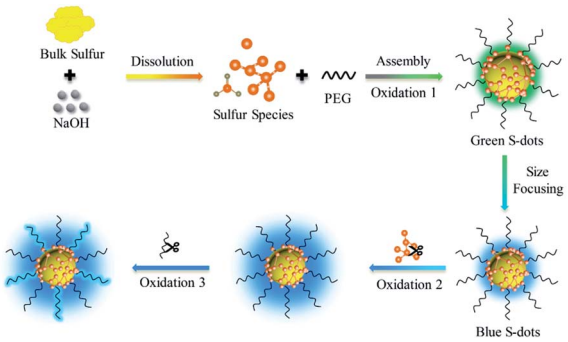

Fig. 4 Schematic illustration of the synthesis and the PL mechanisms of S-dots.

Based on the presented results, the PL of S-dots is attributed to the quantum confinement affected by the surface chemical groups. Fig. 4 demonstrated a relationship between the surface groups, the core, and PL properties. The divalent sulfur ions were oxidized into elemental sulfur by the bubbled O_2 under the passivation of PEG, which formed S-dots, with many sulfur species (S^{2-}, S_x^{2-}, SO_3^{2-}, and SO_4^{2-}) absorbed on the surface. With the decreasing size of the core, the quantum mechanical coupling effect is prominent, generating band structures. This confinement provides the size-dependent bandgap and emission colour to S-dots. The divalent sulfur ions absorbed on the S-dots' surface quench the emission from the sulfur core by providing nonradiative paths. The emission intensity can be promoted by etching those species by O_2 bubbling. PEG is essential for the photoemission of S-dots by stabilization of S-dots. PEG also contributes part of the blue emission from S-dots by the oxidation under alkaline pH.

Conclusions

In summary, we studied the react route and photoemission mechanism of S-dots produced by a mild bubbling-assisted method. The bubbled air is critical for the formation of S-dots, by providing O_2 to transfer divalent sulfur ions into the elemental sulfur core and etching the surface species deactivates nonradiative paths. Experimental evidence shows that the emission depends on the sulfur core and the number of divalent sulfur ions on the surface. Specifically, the emission appears when the exciton relaxes in the sulfur core. The emission colour depends on the S-dot size. The divalent sulfur ions absorbed on the S-dots surface quench the emission, and passivation of the sulfur species by O_2 significantly enhances the PL intensity. Also, a part of the blue emission from S-dots is contributed by the oxidization products of PEG. Overall, we clarify the function of O_2 on the formation and luminescence of S-dots, providing a guide for highly luminescent metal-free QDs for chemical sensing and optoelectronics.

Conflicts of interest

There are no conflicts to declare.

Acknowledgements

This work was financially supported by the National Natural Science Foundation of China (21804030), the outstanding youth project of Natural Science Foundation of Hebei Province (B2020201060), One Hundred Talent Project of Hebei Province (E2019050011), the Natural Science Foundation of Hebei Province (B2020201082), Science and Technology Project of Hebei Education Department (BJ2020033), Natural Science Interdisciplinary Research Program of Hebei University (DXK201906).

References

1 A. Pal, F. Arshad and M. P. Sk, *Adv. Colloid Interface Sci.*, 2020, **285**, 102274.
2 S. Shankar, L. Jaiswal and J.-W. Rhim, *Crit. Rev. Environ. Sci. Technol.*, 2020, 1–28, DOI: 10.1080/10643389.2020.1780880.
3 Z. Wang, C. Zhang, H. Wang, Y. Xiong, X. Yang, Y.-e. Shi and A. L. Rogach, *Angew. Chem., Int. Ed.*, 2020, **59**, 9997–10002.
4 C. Wang, D. Han, J. Wang, Y. Yang, X. Liu, S. Huang, X. Zhang, S. Chang, K. Wu and H. Zhong, *Nat. Commun.*, 2020, **11**, 6428.
5 J. Ning, S. V. Kershaw and A. L. Rogach, *J. Am. Chem. Soc.*, 2019, **141**, 20516–20524.
6 X. Lan, M. Chen, M. H. Hudson, V. Kamysbayev, Y. Wang, P. Guyot-Sionnest and D. V. Talapin, *Nat. Mater.*, 2020, **19**, 323–329.
7 L. Shen, H. Wang, S. Liu, Z. Bai, S. Zhang, X. Zhang and C. Zhang, *J. Am. Chem. Soc.*, 2018, **140**, 7878–7884.
8 H. Wang, Z. Wang, Y. Xiong, S. V. Kershaw, T. Li, Y. Wang, Y. Zhai and A. L. Rogach, *Angew. Chem., Int. Ed.*, 2019, **58**, 7040–7044.
9 S. Li, D. Chen, F. Zheng, H. Zhou, S. Jiang and Y. Wu, *Adv. Funct. Mater.*, 2014, **24**, 7133–7138.
10 Y. Duan, J. Tan, Z. Huang, Q. Deng, S. Liu, G. Wang, L. Li and L. Zhou, *Carbohydr. Polym.*, 2020, **249**, 116882.
11 Y. Sheng, Z. Huang, Q. Zhong, H. Deng, M. Lai, Y. Yang, W. Chen, X. Xia and H. Peng, *Nanoscale*, 2021, **13**, 2519–2526.
12 L. Shen, J. Wei, Z. Liu, Z. Bai, Y. Li, D. Zhang and C. Zhang, *Chem. Mater.*, 2020, **32**, 10476–10481.
13 Y.-e. Shi, P. Zhang, D. Yang and Z. Wang, *Chem. Commun.*, 2020, **56**, 10982–10988.
14 G. Qiao, L. Liu, X. Hao, J. Zheng, W. Liu, J. Gao, C. C. Zhang and Q. Wang, *Chem. Eng. J.*, 2020, **382**, 122907.
15 C. Zhang, P. Zhang, X. Ji, H. Wang, H. Kuang, W. Cao, M. Pan, Y.-e. Shi and Z. Wang, *Chem. Commun.*, 2019, **55**, 13004–13007.
16 Y. Song, J. Tan, G. Wang, P. Gao, J. Lei and L. Zhou, *Chem. Sci.*, 2020, **11**, 772–777.
17 P. Gao, G. Wang and L. Zhou, *ChemPhotoChem*, 2020, **4**, 5235–5244.
18 V. Nasluzov, A. Shor, A. Romanchenko, Y. Tomashevich and Y. Mikhlin, *J. Phys. Chem. C*, 2019, **123**, 21031–21041.
19 Y. He, Y. Qiao, Z. Chang, X. Cao, M. Jia, P. He and H. Zhou, *Angew. Chem., Int. Ed.*, 2019, **58**, 11774–11778.
20 V. Javan Kouzegaran and K. Farhadi, *Micro Nano Lett.*, 2017, **12**, 329–334.
21 W. E. Kleinjan, A. d. Keizer and A. J. H. Janssen, *Water Res.*, 2005, **39**, 4093–4100.
22 H.-L. Wu, L. A. Huff and A. A. Gewirth, *ACS Appl. Mater. Interfaces*, 2015, **7**, 1709–1719.
23 M. Hagen, P. Schiffels, M. Hammer, S. Dörfler, J. Tübke, M. J. Hoffmann, H. Althues and S. Kaskel, *J. Electrochem. Soc.*, 2013, **160**, A1205–A1214.
24 B. Eckert and R. Steudel, in *Elemental Sulfur und Sulfur-Rich Compounds II*, ed. R. Steudel, Springer Berlin Heidelberg, Berlin, Heidelberg, 2003, pp. 31–98, DOI: 10.1007/b13181.
25 R. Steudel, in *Elemental Sulfur und Sulfur-Rich Compounds II*, ed. R. Steudel, Springer Berlin Heidelberg, Berlin, Heidelberg, 2003, pp. 127–152, DOI: 10.1007/b13183.
26 N. Xu and Q. Wen, *Opt. Laser Technol.*, 2021, **138**, 106858.
27 J. Lim, J. Pyun and K. Char, *Angew. Chem., Int. Ed.*, 2015, **54**, 3249–3258.
28 J. Scheirs, S. W. Bigger and O. Delatycki, *Polymer*, 1991, **32**, 2014–2019.
29 K. Nie, X. Wang, J. Qiu, Y. Wang, Q. Yang, J. Xu, X. Yu, H. Li, X. Huang and L. Chen, *ACS Energy Lett.*, 2020, **5**, 826–832.
30 L. Jing, S. V. Kershaw, Y. Li, X. Huang, Y. Li, A. L. Rogach and M. Gao, *Chem. Rev.*, 2016, **116**, 10623–10730.
31 K. Gong, J. E. Martin, L. E. Shea-Rohwer, P. Lu and D. F. Kelley, *J. Phys. Chem. C*, 2015, **119**, 2231–2238.
32 C. Zhang, H. Wang, X. Lan, Y.-e. Shi and Z. Wang, *J. Phys. Chem. Lett.*, 2021, 1413–1420, DOI: 10.1021/acs.jpclett.0c03614.
33 C. M. Thompson, M. Kodaimati, D. Westmoreland, R. Calzada and E. A. Weiss, *J. Phys. Chem. Lett.*, 2016, **7**, 3954–3960.